SEMARAK ILMU PUBLISHING

CFD Letters

Journal homepage:
https://semarakilmu.com.my/journals/index.php/CFD_Letters/index
ISSN: 2180-1363

Secondary Currents at Very Low and High Aspect Ratios of Open Channels

A.-M. Shinneeb[1,*], G. Nasif[1,2], R. Balachandar[2]

[1] Department of Mechanical Engineering, Higher College of Technology, Abu Dhabi, United Arab Emirates
[2] Department of Mechanical, Automotive, and Materials Engineering, University of Windsor, Windsor, Ontario, Canada

ARTICLE INFO

Article history:
Received 16 March 2022
Received in revised form 21 May 2022
Accepted 23 May 2022
Available online 31 May 2022

Keywords:
Secondary currents; turbulence; CFD; IDDES model

ABSTRACT

The present numerical study is an attempt to better understand the effect of the aspect ratio (AR) on the velocity field characteristics of the fully-developed turbulent flow in a straight open channel by contrasting a very low and very high aspect ratio cases (AR = 1 and 12). The AR is defined as the ratio of the width of the channel in a plane normal to the flow direction, to the flow depth. The bulk velocity and water depth considered in this study are 0.75 m/s and 30 mm, respectively, which yield a Reynolds number of Re_H = 22,500. The transient three-dimensional Navier-Stokes equations were numerically solved using a finite-volume approach with improved-delayed detached-eddy simulation (IDDES) turbulence model. The results revealed that the normalized components of the normal stresses by the turbulent kinetic energy *k* are constant over most of the velocity field, although *k* varies in magnitude throughout the velocity field in both AR cases. In addition, the results also revealed a strong anisotropic flow which justifies the formation of secondary currents as a means for transporting the kinetic energy. The results also reveal that both vertical and transverse components of the normal stresses are correlated to the side-recirculation zone (SRZ) and bottom-recirculation zone (BRZ), respectively, which highlights the role of the mean recirculation zones (BRZ & SRZ) in the re-distribution of the turbulent kinetic energy *k* in the velocity field.

1. Introduction

Turbulent flow is a very complex phenomenon, it is one of the most challenging topics in fluid mechanics. Moreover, the presence of solid walls bounding the flow causes the formation of boundary layer, which makes the flow three-dimensional (3D), and thus result in a more intricate flow field due to the wall effect. One of the interesting phenomenon in turbulent flow is the formation of secondary currents. The size and strength of the secondary currents in the flow field depend on different parameters such as the aspect ratio (AR), the flow depth, wall roughness, the distance from the solid boundary, Reynolds number, etc. This phenomenon is usually observed in channel and duct flows. Therefore, understanding the mechanism of these currents is crucial since they affect the characteristics of turbulence and mean flow.

* *Corresponding author.*
Email address: mshinneeb@hct.ac.ae (A.-M. Shinneeb)

https://doi.org/10.37934/cfdl.14.5.115

Open-channel flow is a suitable case to understand the characteristics of the secondary currents. Generally, there are two standard types of secondary currents classified in open-channels [1]. The secondary currents that occur in a straight open channel flow due to turbulence phenomenon is known as Prandtl's second kind, which is the focus of this study. It is reported that the second type of secondary currents occurs due to turbulence anisotropy between velocity components [2]. Nezu and Rodi [3] carried out an experimental study on secondary currents in smooth open-channel flows using a laser-Doppler anemometer (LDA). It was concluded that the secondary current patterns are different from those of duct flows due to the presence of the free-surface. Nezu *et al*., [4] investigated the formation of secondary currents in a smooth rectangular open channel flow by varying the aspect ratio. Shinneeb *et al*., [5] reported the formation of a pair of counter-rotating recirculation zones near the corners of a flume whose size is a function of the AR. One recirculation zone resides above the corner bisector-line which is called the "side-recirculation zone (SRZ)", and the other one resides under the bisector-line which is called the "bottom- recirculation zone (BRZ)". The slope of the line that can be assumed to demarcate the boundary of the recirculation zones in each pair is found to be equal to half of the aspect ratio (AR/2). The size of the BRZ increases with increasing the AR on the expense of SRZ, and both of them become approximately equal in size for AR = 2. Nezu and Nakagawa [6] provided an explanation of the dependence of the secondary currents on the channel AR. In narrow channels (AR < 5), the sidewalls and bed cause an increased anisotropy between fluctuating velocity components, which result in strong secondary currents over the entire channel cross-section. For AR > 10, it is argued that the sidewall effects die out and the flow becomes two-dimensional in the central/core region of the channel. Tominaga *et al*., [7] carried out an experimental study using a hot-film anemometer (HWA) to investigate the secondary currents in rectangular and trapezoidal cross-section open-channel flows. It was concluded that the secondary currents are generated as a result of the anisotropy of turbulence caused by the boundary conditions, and that the secondary currents affect the mean streamwise flow, producing three-dimensional flow. More recently, Nasif *et al*., [8] carried out a computational study using the detached-eddy simulation (DES) turbulent model to investigate the influence of the aspect ratio on the secondary motion in an open-channel flow. The results revealed the formation of two recirculation zones at the top corners near the free surface, whose axes were aligned with the streamwise direction of the flow; in addition to counter-rotating recirculation zones at the bottom corners of the flume.

Even though the secondary currents in turbulent flow have been extensively investigated by numerous researchers, the mechanism that leads to the formation of secondary currents and the influence of the geometry parameters such as the aspect ratio on this formation are still not well understood. This may be attributed to the three-dimensional nature of the turbulent flow and the inherent limitations and high cost of conventional experimental methods, which limits their effectiveness in such studies compared to numerical approaches. The availability of enhanced computational tools makes the investigation of the secondary currents in the flow field more efficient. Thus, the objective of this study is to enhance our understanding of the effect of the AR on the formation of secondary currents in a smooth open-channel flow using a numerical approach. This is achieved by contrasting the mean velocity field and turbulence characteristics at low and high AR. Two aspect ratio cases are investigated in this study; a narrow case of AR = 1 and a wide case of AR =12. A three-dimensional time-dependent improved-delayed detached-eddy simulation (IDDES) turbulent model is used in the study. The purpose of this study is to provide a deeper understanding of the effect of the aspect ratio (AR) on the formation of secondary currents that is not possible by experimental approaches, since this phenomenon is observed in a variety of engineering and/or environmental applications. This objective is achieved in this study by investigating the mean velocity field and turbulence quantities.

2. Model Setup and Boundary Conditions

A schematic diagram of the open channel flow that illustrates the computational domain and the relevant boundary conditions that have been employed in this study are shown in Figure 1. In this figure, *x*, *y*, and *z* represent the streamwise, vertical, and transverse directions, respectively. In this study, the streamwise length *L* and water layer depth *H* are 500 mm and 30 mm, respectively, for both cases; while the channel widths *B* = 30 and 360 mm are used to produce the desired aspect ratios AR = 1 and 12, respectively. The aspect ratio (AR), which is the main parameter in this study, is determined by the ratio of the horizontal width *B* of the rectangular channel cross-section to the water layer depth *H*. Thus, the computational domain adopted in this study extends from 0 to *L* in the streamwise direction *x*, from 0 to *H* in the vertical direction *y*, and from –*B*/2 to *B*/2 in the transverse direction *z*. As illustrated in Figure 1, all wall boundaries in contact with the water region (labelled with letter "b") are considered as a no-slip smooth boundary, while the top free surface (labelled with letter "a") is treated as a slip boundary. The fully-developed turbulent velocity profile, which is used as an inlet boundary condition (labelled with letter "d" in Figure 1), is obtained as described in section 3; while the outflow boundary (labelled with letter "c") is treated as an atmospheric pressure. The bulk velocity at the inlet of the channel is 0.75 m/s, which yields a Reynolds number Re_H, based on the water depth *H*, of 22,500. Since the purpose of this study is to understand the secondary flow as a turbulent phenomenon that occurs in open channels, the magnitude of Re considered in this study can meet the objective of the current study.

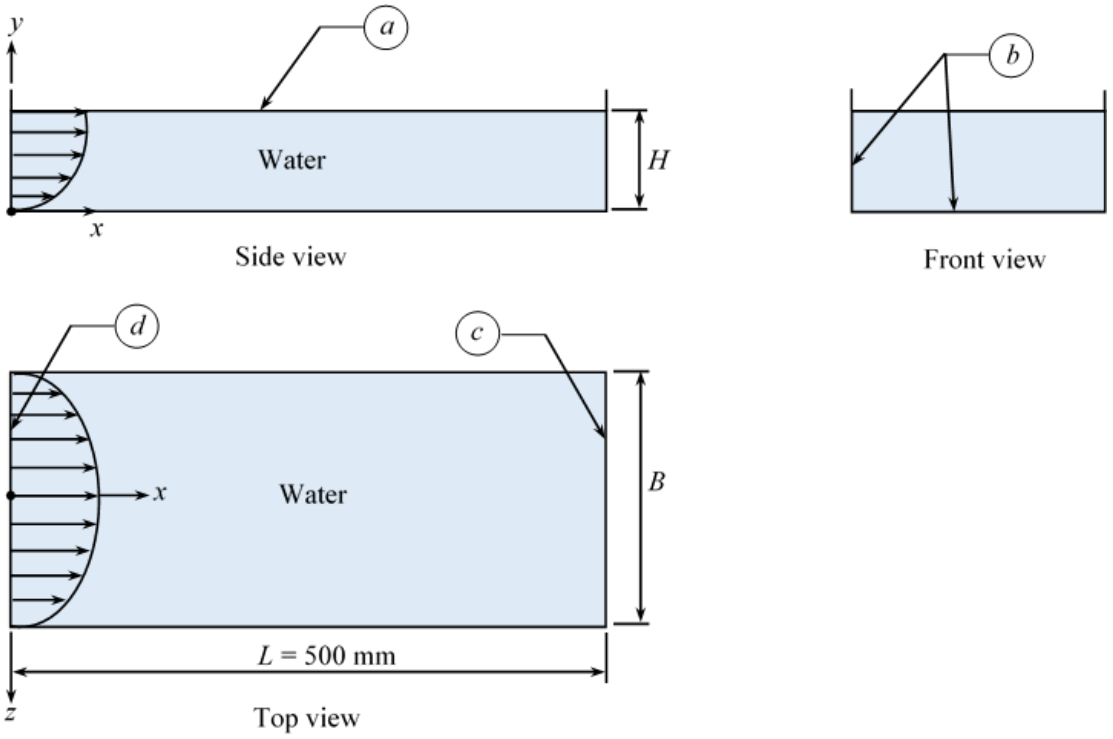

Fig. 1. A schematic diagram of the open channel flow that shows the computational domain with the relevant boundary conditions employed in this study. In this diagram, *a* represents slip boundary; *b* represents no-slip boundary; *c* represents outlet boundary; and *d* represents fully-developed inlet velocity

3. Computational Methodology

The open channel flow is simulated using Siemens PLM's STAR-CCM+ [9] with a structured trimmer mesh. The trimmer meshing model utilizes a template mesh that is constructed from hexahedral cells is used to mesh the computational domain. First-order implicit marching in time and second-order differencing in space are used to discretize the governing equations. Since the problem in the current study is characterized by mostly low frequency effects, the first order time discretization is sufficient to generate results with good accuracy. The time-dependent governing equations comprise a continuity equation for conservation of mass and three conservation of momentum equations. Each of these equations can be expressed in a general form by the transport of a specific scalar quantity ϕ per unit mass, represented in a continuous integral form as [10]:

$$\frac{\partial}{\partial t}\int_{\mathrm{CV}} \rho\phi d\mathrm{V} + \oint_A \mathbf{n}\cdot(\rho\phi\mathbf{u})dA = \oint_A \mathbf{n}\cdot\left(\Gamma_\phi \boldsymbol{\nabla}\phi\right)dA + \int_{\mathrm{CV}} S_\phi \, d\mathrm{V} \tag{1}$$

where CV in Eq. (1) represents the three-dimensional control volume over which the volume integration is carried out, *A* is the bounding surface of the control volume. The terms in Eq. (1) from left to right are the rate of change of the total quantity of the fluid property ϕ in the control volume, the rate of change of the property ϕ due to the convection flux across the bounding surface of the control volume, the rate of change of the property ϕ due to the diffusive flux across the bounding surface of the control volume, and the volumetric source in the control volume. The unit vector **n** in Eq. (1) is the outward normal vector to the surface, **u** is the instantaneous velocity vector, ρ is the density, and Γ_ϕ is the diffusion coefficient.

The present computational study of a straight open turbulent channel flow was carried out by using the improved-delayed detached-eddy simulation (IDDES) turbulent model (see [11-13]). It is a modified turbulent model that employs Reynolds-Averaged Navier–Stokes (RANS) equation at the near-wall regions and Large-eddy simulation (LES) at the rest of the flow domain. The model was originally formulated by replacing the distance function in the Spalart-Allmaras model with a modified distance function. The *k*-ε Shear Stress Transport (SST) turbulence model is a two-equation eddy-viscosity model [14, 15] and has been selected as the RANS part of the IDDES turbulence model in this study. The *k*-ε SST model solves additional transport equations for turbulent kinetic energy *k* and specific dissipation rate ε, from which the turbulent kinematic viscosity ($\nu_t = k/\varepsilon$) can be derived. The transport equations of *k* and ε are described in Ref. [15].

The solution procedures may be summarized as follows. In the beginning of the simulation, the flow velocity at the inlet of the channel is assumed to be uniform with a magnitude of 0.75 m/s. The corresponding Reynolds number based on the water depth *H* is Re_H = 22,500. The transient three-dimensional Navier-Stokes equations were numerically solved for all nodes in the computational domain simultaneously using a finite-volume approach with improved-delayed detached-eddy simulation (IDDES) turbulent model. The mean velocity field is then calculated from the results. The computational process continued until the fully-developed velocity profile was achieved, where the inlet boundary was updated for each computational cycle by mapping the mean velocity profile from the *y*-*z* plane located at the streamwise location *x*/*L* = 0.5 of the channel (see Figure 1) to the inlet boundary (*x*/*L* = 0). The iteration is terminated for each cycle when the maximum difference between the mean velocities and turbulence quantities obtained from the current and previous stages satisfies the convergence criterion ($< 10^{-6}$). Once the fully-developed velocity profile is achieved, it is extracted from the streamwise location *x*/*L* = 0.5 of the channel and then mapped to the inlet boundary at *x*/*L* = 0 for generating the instantaneous velocity (*u*, *v*, & *w*) field for 10 s, which was used for calculating the time-averaged velocity field and turbulence quantities (see Nasif *et al*., [8] for more details).

4. Mesh Generation

In the present study, structured-trimmer elements are used to mesh the computational domain. The advantage of structured meshing over unstructured meshing is the ability of the user to have better control of interior node locations and cell sizes. This leads to more accurate results and better convergence in the computational fluid dynamics (CFD) solvers. The verification of the reliability of the current study was carried out in two stages. The first stage was the selection of optimum grid size. This objective was achieved by carrying out a grid independence study. Four different sets of grid sizes in the computational domain (varied by increasing the number of grids) were tested for the aspect ratio AR = 12 case to find out their effect on the mean velocity field and turbulence quantities in the fully developed region of the channel flow. It has been found that the change of the mean quantities becomes relatively small beyond a number of cells of approximately 9×10^6. The corresponding normalized grid size (defined as the ratio of the third-root of the cell volume $V^{1/3}$ to the water depth H) is found to be in the range of 4.2×10^{-5} –1.25×10^{-3}. Accordingly, this range of cell sizes is used for all AR cases. In this study, the total number of cells used for the computation is 1.3 and 8.7 million elements for AR = 1 and 12, respectively. More information about the meshed domain and grid independence study may be found in Nasif *et al*., [8, 16-18]. In summary, ten layers of fine prism cells, packed within 1.5 mm using a stretching factor of 1.5, are employed in this study to resolve the wall effects. Based on the dimensionless wall-normal distance y^+, the size of the first prism layer adjacent to the wall is small enough so that the dimensionless wall-normal distance y^+ of the first layer is smaller than two everywhere near the wall, which indicates that the viscous sublayer is captured in the simulation (see Nasif [19] for more details).

The second stage of verification was performed by comparing the mean velocity and turbulence quantities obtained from this simulation with the experimental studies of Heidari *et al*., [20], which were carried out using the particle image velocimetry (PIV) system in a recirculating open-channel flume at the Hydraulic Engineering Research Laboratory at the University of Windsor. The comparison revealed that the maximum difference between the numerical and experimental results for the mean streamwise U and transverse velocities W as well as the Reynolds stress $\langle uw \rangle$ was less than 15%. A complete discussion of the data validation can be found in Nasif *et al*., [16, 17].

Another important aspect for reliable numerical results is the selection of the time step. The time step should be selected based on the local Courant–Friedrichs–Lewy (CFL) condition (Courant number ≤1.0) to ensure numerical stability [21]. Different time steps were investigated by searching for a time step that makes the difference between the mean velocity profiles (along the vertical and transverse planes) almost independent of the time step. Consequently, the final time step that satisfies this condition is 0.2 ms, which yields a Courant number less than 0.5 in the entire computational domain (see Nasif *et al*., [8] for more information). Five internal iterations were employed at each time step. Finally, the time used for calculating the time-averaged velocity field and turbulence quantities after reaching the fully developed flow state is 10 s.

5. Results and Discussions

In this section, vector plots and/or colour contours of the mean velocity field of an open channel flow are presented and discussed. Two cases are discussed in this study to highlight the effect of aspect ratio (AR) on the formation of secondary currents; one represents a small aspect ratio (AR =1) and the other one represents a much larger aspect ratio (AR = 12), which is used as a reference case. In the following results, x-, y-, and z-axes represent streamwise, vertical, and horizontal locations respectively; while U, V, and W represent the corresponding mean velocity components. It should be

noted that the computational results of the open channel flow presented in sections 5.1-5.3 were already discussed in Shinneeb *et al*., [5, 22], and is presented here for completeness.

5.1 Boundary Layer Characteristics

Figure 2 shows the distribution of the streamwise component of the mean velocity U in the channel flow for AR = 12 in terms of the dimensionless wall velocity U^+ (= u/u_τ) and vertical axis y^+ (= yu_τ/v). The present velocity profile is compared with the experimental results of Heidari *et al*., [20] for smooth channel flow at a similar Reynolds number. The present results are in very good agreement with the previous channel flow data.

The boundary layer thickness δ (perpendicular to the bed) in this study is estimated based on $0.995U_b$, and found to occupy ~29.3% of the water layer depth H. Consequently, the displacement thickness δ^* and momentum thickness ϑ were estimated to be 0.58 and 0.41 mm, respectively. The resulting shape factor is 1.41 and the Reynolds number based on the momentum thickness Re_ϑ is ~308. The friction velocity u_τ, defined as $\sqrt{\tau/\rho}$, is determined by the Clauser chart method [23], which is based on the assumption that the velocity profile follows a universal logarithmic form in the overlap region of the boundary layer. In this study, the friction velocity u_τ is estimated to be 39 mm/s. The corresponding skin friction coefficient C_f, defined by $2(u_\tau/U_b)^2$, is found to be 5.41×10^{-3}. The viscous length scale l_v, defined by (v/u_τ, where v is the kinematic viscosity of the water) is estimated to be 0.026 mm.

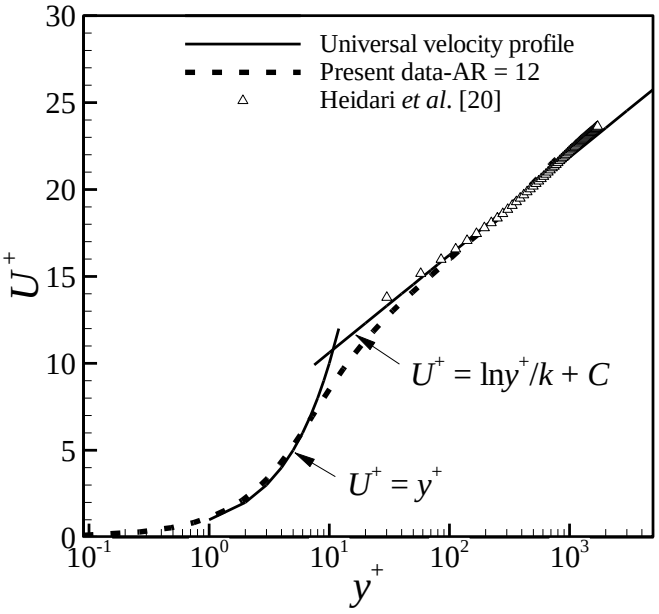

Fig. 2. Mean streamwise velocity distribution of the smooth open-channel flow using the inner coordinate. The current velocity data for AR = 12 is compared with experimental results

5.2 Mean Velocity Field

Figure 3 shows two vector plots of the mean velocity field in *y*-*z* plane for aspect ratios AR = 1 and 12, respectively, extracted from the fully-developed flow region of an open channel flow. In these plots, the colour contour, which represents the mean streamwise velocity component, is also shown in the plots to provide a better description of three-dimensional (3D) velocity field. In this figure, locations are normalized by the water layer depth H and velocities are normalized by the bulk velocity

U_b. Note that only some vectors are shown to avoid cluttering on the figures. The vector plot shown in Figure 3(a) illustrates clearly the formation a pair of strong counter-rotating recirculation zones near the bottom corners of the channel for the AR = 1 case, whose axes are aligned with the streamwise direction *x*; one of the pair resides near the bottom bed while other one is relatively bigger and resides near the sidewalls. Furthermore, there is a strong downward flow in the mid-vertical plane driven by the recirculation zones that reside near the sidewalls which meets with a relatively weaker upward flow driven by the lower recirculation zones. Figure 3(b) shows that the behaviour of the AR = 12 case is very different. It shows the formation of a pair of counter-rotating recirculation zones in the bottom corners of the channel. However, the strengths of the recirculation zones near the bed are quite energetic and they appear to span almost the whole flow depth, while the zones that reside near the sidewalls appear weak and confined in a narrow region near the sidewalls (see the region highlighted by a red square). In the core region of this wide channel (AR = 12), Figure 3(b) shows that the magnitude of the mean vertical *V* and horizontal *W* velocity components are almost zero. On the other hand, the colour contour generally illustrates that the mean streamwise velocity is zero at the solid walls and increase gradually to reach its maximum magnitude in the core region of the channel flow for AR = 1 and 12 as shown in Figures 3(a) and 3(b). However, the darker brown colour in the core region of Figure 3(a) compared to Figure 3(b) indicates that the magnitude of *U* for AR = 1 is larger than the AR = 12 case. This may be attributed to the formation of the boundary layers on the solid bottom and side walls, which displaces the flow vertically and horizontally, respectively, and thus enhance *U*.

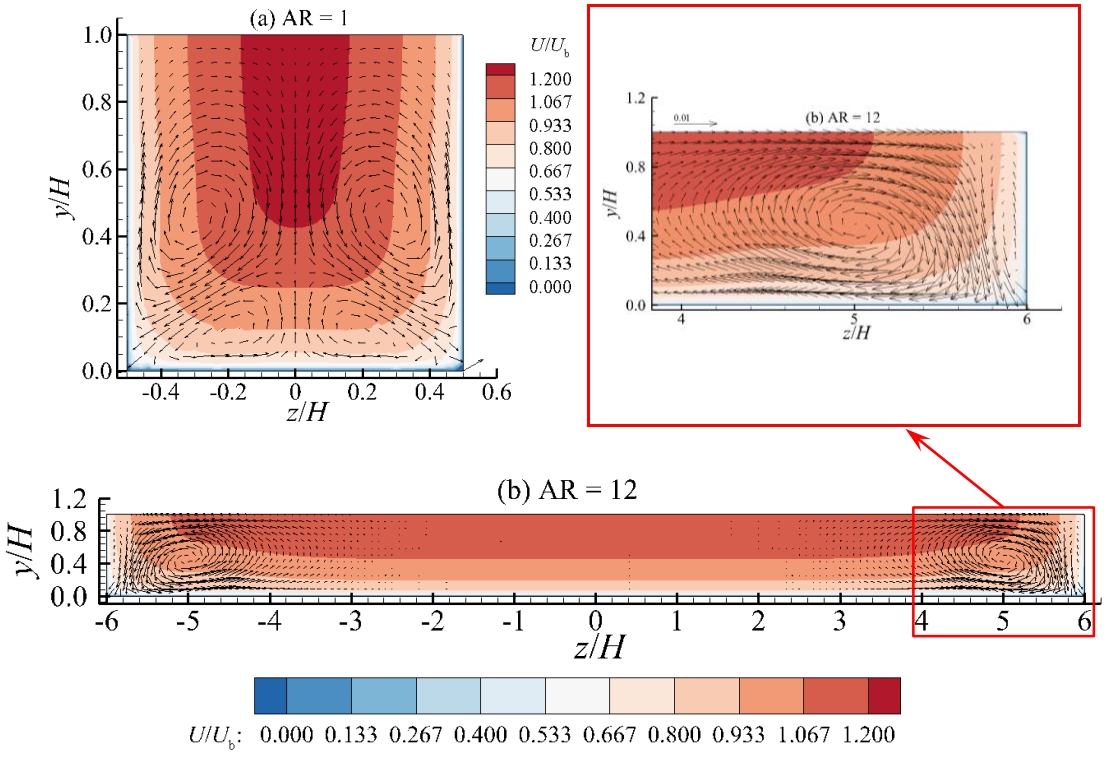

Fig. 3. Mean velocity field for an open channel flow in the fully-developed flow region for (a) AR = 1 and (b) AR = 12. The colour contour represents the normalized mean streamwise velocity U/U_b component. This figure is reproduced from Shinneeb *et al*., [22] with the permission of WIT Press (doi:10.2495/MPF210051)

5.3 Mean Turbulent Kinetic Energy

To highlight the effect of the aspect ratio on the energy distribution in the flow, Figure 4 displays the turbulent kinetic energy *k* as a colour contour superimposed on the mean velocity field in *y*-*z* plane. In this figure, *k* is normalized by U_b^2. Figures 4(a) and 4(b) illustrate that the maximum turbulent kinetic energy *k* occurs in the layer adjacent to the bottom and side walls (brown colour), while the minimum *k* occurs in the core region of the flow far from the solid walls (blue colour). This increase in *k* near the solid walls is due to the velocity gradient of *U* & *V* (near the side walls) and *U* & *W* (near the bottom wall), which produces a strain field that enhances the velocity fluctuations (u', v', and/or w'), and hence the turbulent kinetic energy *k*. According to Figure 4, the mechanism that governs the re-distribution of *k* throughout the velocity field is the recirculation zones (SRZ and BRZ) whose spatial size/influence depend on the AR. Hence, the vertical orientation of minimum *k* near the vertical mid-plane for AR = 1 and the horizontal orientation of minimum *k* parallel to the free surface for AR = 12 is due to the dominance of either SRZ or BRZ in these cases, respectively.

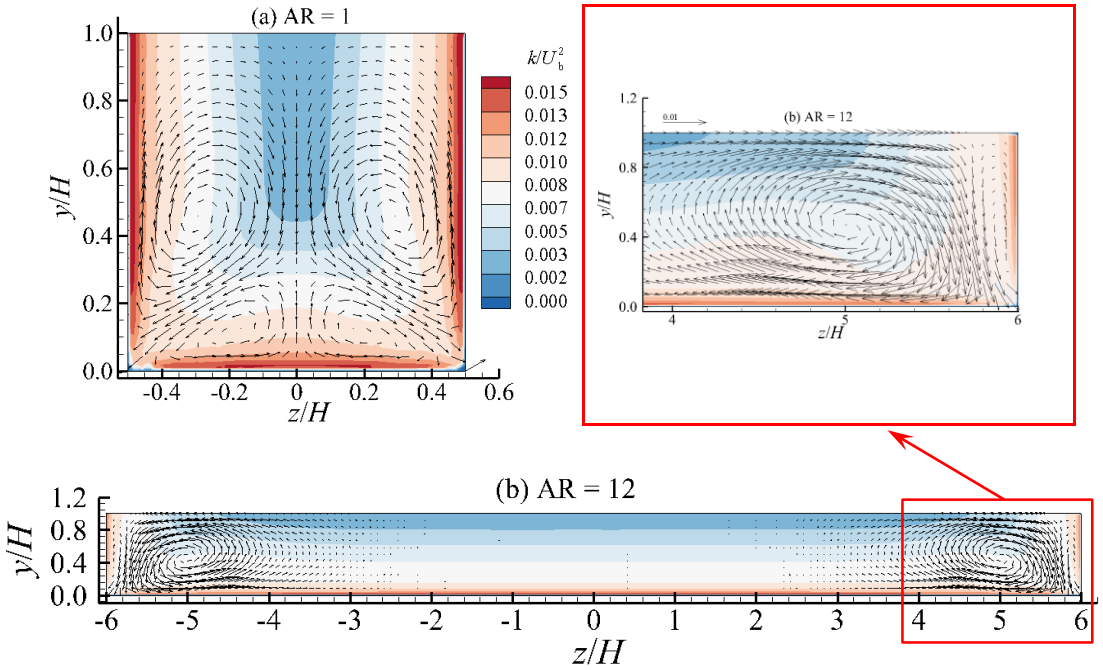

Fig. 4. Mean velocity field for an open channel flow in the fully-developed flow region for (a) AR = 1 and (b) AR = 12. The colour contour represents the normalized turbulent kinetic energy k/U_b^2. This figure is reproduced from Shinneeb *et al*., [22] with the permission of WIT Press (doi:10.2495/MPF210051)

5.4 Normal Stress Parameters

The distribution of the normal streamwise u_{rms}^2, vertical v_{rms}^2, and transverse w_{rms}^2 turbulence stress components throughout the *y*-*z* plane in the fully-developed region of the channel flow is displayed in Figures 5, 6, and 7. Each figure consists of two colour contour plots of the normal turbulence stress (u_{rms}^2, v_{rms}^2, or w_{rms}^2) for AR = 1 and 12 superimposed on the mean velocity field. In these plots, locations *y* and *z* are normalized by the water depth *H* and the stresses are normalized by the turbulent kinetic energy 2*k*. The purpose of normalizing by 2*k* is to highlight the degree of anisotropy of the turbulence components in a scale of 0 to 1. It should be noted that only half of the

plots for AR = 12, which represent the right side (+*z*/*H*), is displayed in these figures due to the symmetry of the velocity fields and space limitation.

Figure 5 illustrates clearly that $u_{\mathrm{rms}}^2/2k$ is uniform over most of the velocity field with a magnitude of approximately 0.52 for both cases although the magnitude of *k* is not uniform throughout the velocity fields as shown in Figure 4. However, the magnitude of $u_{\mathrm{rms}}^2/2k$ appears to gradually increase to approximately 0.90 in a thin layer of thickness 0.1*H* adjacent to the wall boundaries. On the other side, $u_{\mathrm{rms}}^2/2k$ appears smaller (≈ 0.47) in a relatively thin region oriented vertically parallel to the mid-vertical plane for AR = 1, and horizontally parallel to the free surface for AR = 12. The uniform distribution of $u_{\mathrm{rms}}^2/2k$ is interesting since it indicates that the ratio of this streamwise component is constant regardless of the magnitude of *k*. In other words, this result indicates that the variation of v_{rms}^2 and w_{rms}^2 are very small compared to the variation of u_{rms}^2, and thus the ratio depends mainly on the streamwise component in the numerator and the denominator.

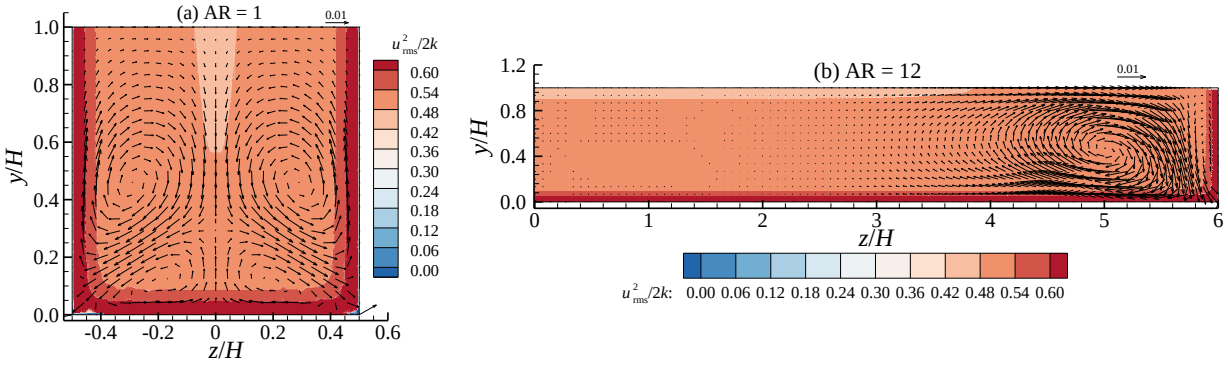

Fig. 5. Colour contour represents the distribution of the normalized streamwise stress $u_{\mathrm{rms}}^2/2k$ superimposed on the mean velocity field for an open channel flow in the *y*-*z* plane for (a) AR = 1 and (b) AR = 12

The distribution of the stresses $v_{\mathrm{rms}}^2/2k$ and $w_{\mathrm{rms}}^2/2k$ throughout the velocity field in *y*-*z* plane for AR = 1 and 12 is shown as a colour contour in Figures 6 and 7. Similar to the $u_{\mathrm{rms}}^2/2k$ results, the distribution of $v_{\mathrm{rms}}^2/2k$ in Fig. 6 and $w_{\mathrm{rms}}^2/2k$ in Figure 7 also appears uniform over most of the velocity field, which suggest a strong correlation between the velocity fluctuations u' & v' and u' & w' (i.e. an increase in one component is associated with a decrease in the other component to conserve *k*); while v' & w' seems to be uncorrelated as will be shown later. In addition, Figures 6 and 7 show that $v_{\mathrm{rms}}^2/2k$ and $w_{\mathrm{rms}}^2/2k$ are correlated to the recirculation zones (BRZ & SRZ). The magnitude of $v_{\mathrm{rms}}^2/2k$ and $w_{\mathrm{rms}}^2/2k$ is generally smaller than one-third for both the AR cases, which reveals the anisotropic nature of the flow. However, the decrease of the AR appears to slightly enhance $v_{\mathrm{rms}}^2/2k$ and inhibit $w_{\mathrm{rms}}^2/2k$ over most of the velocity field as reflected by the colour level. The plots illustrate that both v_{rms}^2 and w_{rms}^2 are correlated to the SRZ and BRZ, respectively, and the increase in the size of SRZ is associated with an increase in $v_{\mathrm{rms}}^2/2k$, and vice versa for $w_{\mathrm{rms}}^2/2k$. This observation highlights the role of the mean recirculation zones (BRZ & SRZ) in the re-distribution of the turbulent kinetic energy *k* in the velocity field.

To highlight the effect of the AR on the re-distribution of the turbulent kinetic energy *k*, both $v_{\mathrm{rms}}/u_{\mathrm{rms}}$ and $w_{\mathrm{rms}}/u_{\mathrm{rms}}$ are plotted as a colour contour in Figure 8. It is interesting to see that the strength of v_{rms} is associated with the SRZ as shown by the colour level in Figures 8(a) and 8(b); while the strength of w_{rms} is associated with the BRZ as shown in Figures 8(c) and 8(d). In other words, the decrease of the AR enhances the vertical velocity fluctuations v' as a result of the spatial expansion of the SRZ as shown in Figure 8(a) on the expense of the BRZ. Similarly, there is an enhancement in the transverse velocity fluctuations w' with increasing the AR as shown in Figure 8(d). However, it

can be observed that the magnitude of w_{rms}/u_{rms} is approximately equal to v_{rms}/u_{rms} in the near free-surface region oriented vertically parallel to the vertical mid-plane (z/H = 0) for AR = 1 (see Figures 8a & 8c). Considering that the streamwise velocity fluctuations u' is minimum in this region, the relatively high values of v_{rms}/u_{rms} and w_{rms}/u_{rms} in this region is an indication of the transfer of energy from this component to the vertical and transverse components.

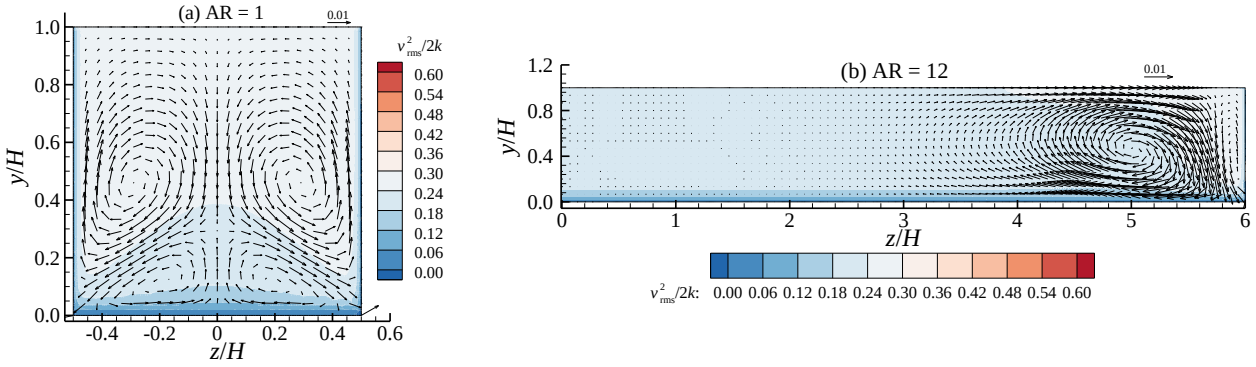

Fig. 6. Colour contour represents the distribution of the normalized vertical stress $v^2_{rms}/2k$ superimposed on the mean velocity field for an open channel flow in the *y-z* plane for (a) AR = 1 and (b) AR = 12

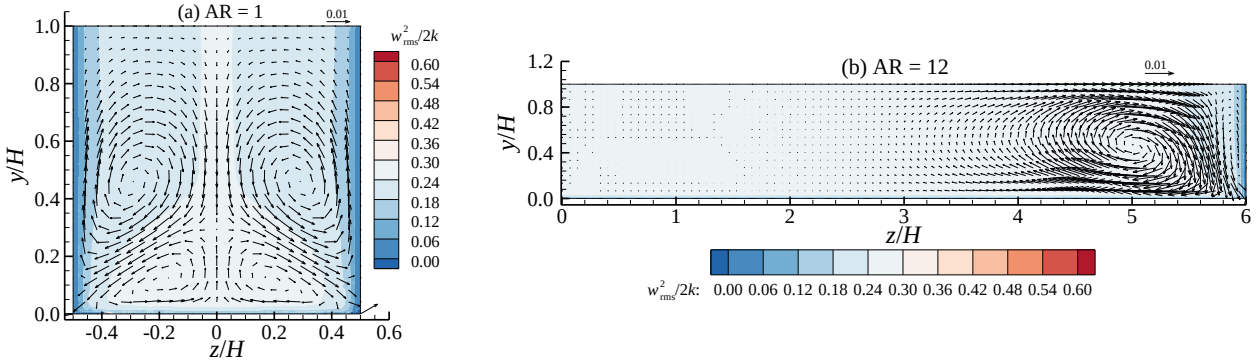

Fig. 7. Colour contour represents the distribution of the normalized transverse stress $w^2_{rms}/2k$ superimposed on the mean velocity field for an open channel flow in the *y-z* plane for (a) AR = 1 and (b) AR = 12

In summary, the ratios v_{rms}/u_{rms} and w_{rms}/u_{rms} are generally smaller than 0.8, which confirms the anisotropy of the current turbulent flow. The imbalance in the turbulent kinetic energy necessitates the transfer of the energy from one component to another component by either the SRZ or BRZ based on the AR.

5.5 Reynolds Shear Stress

The distribution of the Reynolds shear stress $< uv >/k$, $< uw >/k$, and $< vw >/k$ in the fully-developed channel flow is presented as a colour contour superimposed on the vector plot in Figures 9, 10, and 11. The purpose of these plots is to shed light on the regions of strong/weak correlation between the velocity fluctuations (u' & v', u' & w', and v' & w') compared to the total turbulent kinetic energy *k*.

To have a better perception of the results, it should be noted that the ejection and sweep events that occur near the bed are represented by negative <*uv*>, and outward and inward interactions by positive <*uv*>. For the right-side wall, the ejection and sweep events are represented by positive

<*uw*>, while the events' sign is reversed for the left-side wall. Figure 9 displays the colour contour plots of $< uv >/k$ on the *y-z* plane velocity field for AR = 1 and 12. These plots show that the distribution of <*uv*>/*k* is negative (blue colour) and appears dominant in the near-bed region, which suggests the frequent occurrence of ejection/sweep events; while positive <*uv*> (brown colour) is absent. Moreover, Figure 9(b) shows that the negative <*uv*> region near the bed is more dominant for AR = 12. As discussed earlier, the increase in the magnitude of <*uv*>/*k* suggests that the velocity fluctuations (*u'* and *v'*) become more correlated with increasing the AR, which is tied to the decrease in the size of the bed recirculation zone (BRZ).

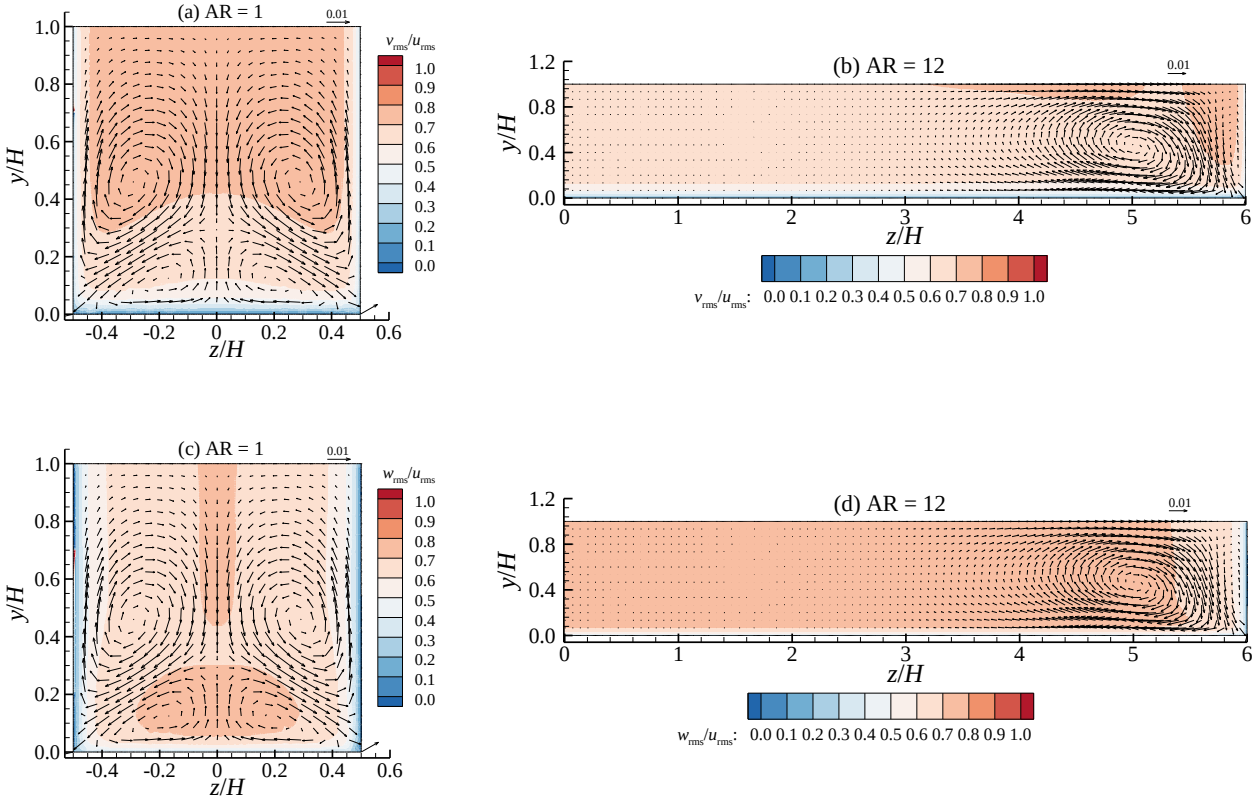

Fig. 8. Colour contour which represents the distribution of $v_{\mathrm{rms}}/u_{\mathrm{rms}}$ and $w_{\mathrm{rms}}/u_{\mathrm{rms}}$ superimposed on the mean velocity field for an open channel flow in the *y-z* plane for AR = 1 (a & c) and AR = 12 (b & d), respectively

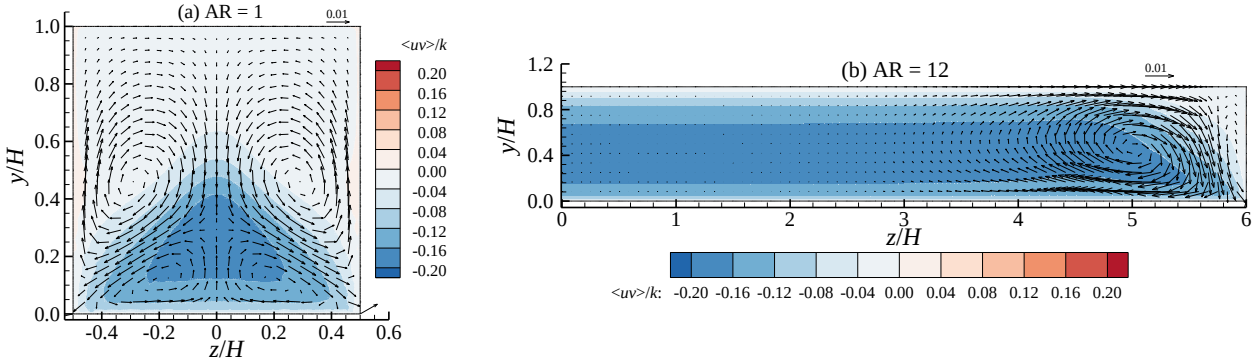

Fig. 9. Colour contour that represents the distribution of the normalized Reynolds shear stress $< uv >/k$ superimposed on the mean velocity field for an open channel flow in the *y-z* plane for (a) AR = 1 and (b) AR = 12

Figure 10 shows the distribution of the Reynolds shear stress $< uw >/k$ for AR = 1 and 12. These plots illustrate that <*uw*> is positive (brown colour) in the right side (+*z*/*H*) and negative (blue colour) in the left side. Once again, the colour contour indicates the dominance of ejection/sweep events in both sides of the channel flow. It is interesting to see that the spatial extent of <*uw*> is correlated with the side recirculation zone (SRZ), which expands with decreasing the AR as shown in Figure 10(a). For the AR = 12 case, the correlation of the velocity fluctuations (*u'* and *w'*) appears very weak. Conversely, the correlation of the velocity fluctuations (*v'* and *w'*), shown in Figure 11, appears very weak compared to the Reynolds stress results presented in Figures 9 and 10.

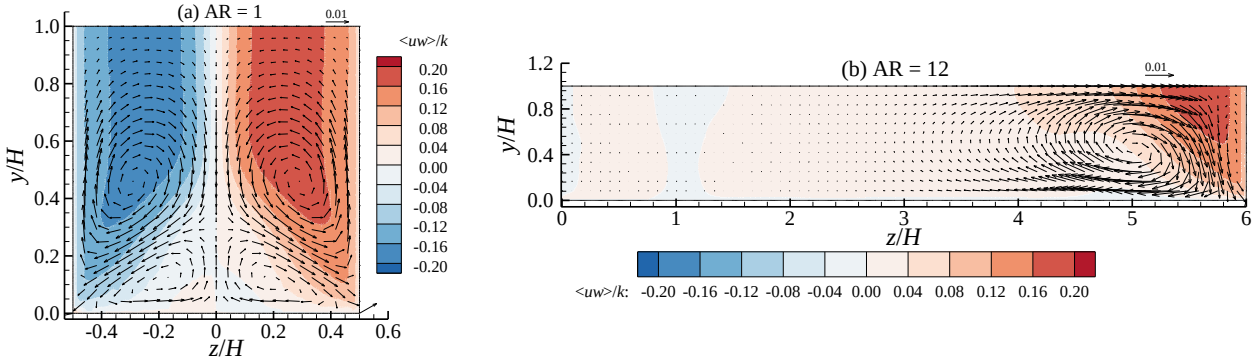

Fig. 10. Colour contour represents the distribution of the normalized Reynolds shear stress $< uw >/k$ superimposed on the mean velocity field for an open channel flow in the *y*-*z* plane for (a) AR = 1 and (b) AR = 12

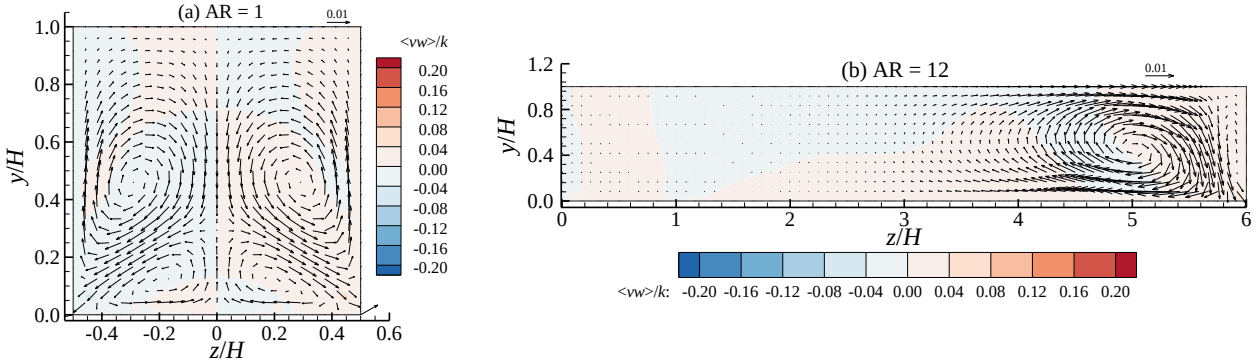

Fig. 11. Colour contour that represents the distribution of the normalized Reynolds shear stress $< vw >/k$ superimposed on the mean velocity field for an open channel flow in the *y*-*z* plane for (a) AR = 1 and (b) AR = 12

To visualize the regions of dominance of each component of the Reynolds shear stress, Figure 12 shows the colour contour of <*uv*>/<*uw*> and <*vw*>/<*uw*> superimposed on the mean velocity field for an open channel flow in the *y*-*z* plane for AR = 1 and 12. It should be noted that the sign of <*uv*> near the bottom solid wall is negative as displayed in Figure 9 and, hence, the positive magnitude of <*uv*>/<*uw*> is due to the negative sign of <*uw*>. Figure 12(a) illustrates that the magnitude of <*uv*> is larger than the magnitude of <*uw*> in the region of induced flow by the SRZ and BRZ for AR = 1 as reflected by the dark blue and brown colours. However, the white region, located near the bottom solid wall at the sides of the vertical mid-plane (*z*/*H* = 0), which is a masked area, represents a very large magnitude of the ratio (<*uv*>/<*uw*> >> 10) because <*uw*> approaches zero in this region. For the remaining of the velocity field, the magnitude of <*uv*>/<*uw*> is relatively small, which indicates weak momentum exchange by <*uv*> and strong momentum exchange by <*uw*> in these regions (see Figure

10). The effect of the AR can be observed by comparing plots (i) and (ii) in Figure 12(a), which reveals the expansion of <*uv*> throughout the velocity field with increasing the AR as a result of the expansion of the BRZ; and vice versa for the AR = 1.

On the other side, Figure 12(b) shows the distribution of <*vw*>/<*uw*> for AR = 1 and 12. It is clear that the magnitude of <*vw*> is very small compared to <*uw*>, which indicates a very weak correlation between v' & w'. However, there is an enhancement in the correlation between v' & w' (albeit small) in the region where the induced upward flow by the BRZ meets with the downward flow by the SRZ (the region of dark brown colour in plot i) for AR = 1. For AR = 12, the magnitude of <*vw*> is relatively small compared with <*uw*>. Note that the dark brown/blue colour shown in the region z/H < 1.6 in plot (ii) for AR = 12 is due the negligible magnitude (almost zero) of <*uw*> and should be ignored.

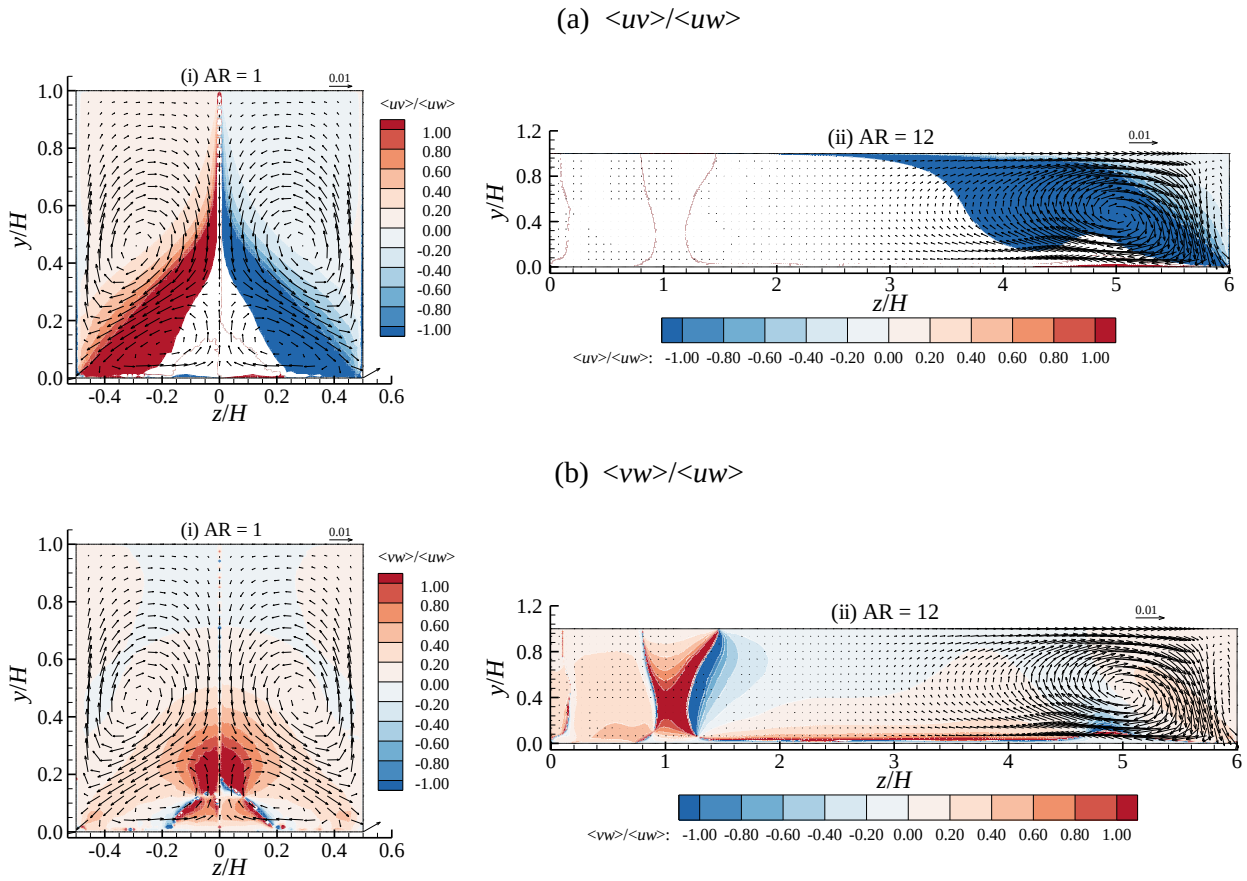

Fig. 12. Colour contour that represents the ratio of the Reynolds shear stress (a) <*uv*>/<*uw*> and (b) <*vw*>/<*uw*> superimposed on the mean velocity field for an open channel flow in the *y*-*z* plane for AR = 1 and 12

6. Conclusions

The present numerical study is an attempt to better understand the effect of the aspect ratio (AR) on the velocity field characteristics of the fully-developed turbulent flow of a straight open channel by contrasting a very low and very high aspect ratio cases (AR = 1 and 12). The bulk velocity U_b and water depth H considered in this study are 0.75m/s and 30 mm, respectively, which yield a Reynolds number of Re_H = 22,500. The following conclusions may be drawn from the results:

I. Although the magnitude of the turbulent kinetic energy k varies throughout the velocity field for AR = 1 and 12, the normalized streamwise component $u_{\mathrm{rms}}^2/2k$ is constant over most of

the velocity field with a magnitude of approximately 0.52. Similarly, the distribution of $v_{\mathrm{rms}}^2/2k$ and $w_{\mathrm{rms}}^2/2k$ also appears uniform over most of the velocity field, which suggest a strong correlation (i.e. an increase in one component is associated with a decrease in the other component to conserve *k*) between the velocity fluctuations u' & v' and u' & w'; while v' & w' appears almost uncorrelated.

II. The magnitude of the vertical $v_{\mathrm{rms}}^2/2k$ and transverse $w_{\mathrm{rms}}^2/2k$ components of the normal stresses is generally smaller than one-third in each AR case, which reveals the anisotropic nature of the flow and justifies the formation of secondary currents as a means for transporting the kinetic energy. However, the decrease of the AR appears to slightly enhance $v_{\mathrm{rms}}^2/2k$ and inhibit $w_{\mathrm{rms}}^2/2k$ over most of the velocity field. The results also reveal that both v_{rms}^2 and w_{rms}^2 are correlated to the side-recirculation zone (SRZ) and bottom-recirculation zone (BRZ), respectively (i.e. the increase in the size of SRZ is associated with an increase in v_{rms}^2, and vice versa for w_{rms}^2). This observation highlights the role of the mean recirculation zones (BRZ & SRZ) in the re-distribution of the turbulent kinetic energy *k* in the velocity field.

III. The distribution of the Reynolds shear stress <*uv*>/*k* is negative and appears dominant in the near-bed region, which suggests the frequent occurrence of ejection/sweep events; while positive <*uv*> is absent. Moreover, the negative <*uv*> region near the bed is more dominant for AR = 12. This behavior suggests that the velocity fluctuations (*u'* and *v'*) become more correlated with increasing the AR, which is tied to the decrease in the size of the BRZ.

IV. The momentum exchange by <*uv*> is relatively weaker than the momentum exchange by <*uw*>, while momentum exchange by <*vw*> is negligible due to a very weak correlation between v' & w'. In addition, the increase of the AR leads to the expansion of <*uv*> at the expense of <*uw*> throughout the velocity field as a result of the expansion of the BRZ; and vice versa for the AR = 1. For <*vw*>, there is a slight enhancement in the correlation between v' & w' for the low AR in the meeting region of the induced flow by the BRZ and the SRZ

Acknowledgements

The support of Natural Sciences and Engineering Research Council (NSERC) of Canada is gratefully acknowledged. This research was made possible by the facilities of the Shared Hierarchical Academic Computing Network (SHARCNET: www.sharcnet.ca) and Compute/Calcul Canada.

References

[1] Bradshaw, Peter. "Turbulent secondary flows." *Annual review of fluid mechanics* 19, no. 1 (1987): 53-74. https://doi.org/10.1146/annurev.fl.19.010187.000413

[2] Einstein, Hans Albert, and Huon Li. "Secondary currents in straight channels." *Eos, Transactions American Geophysical Union* 39, no. 6 (1958): 1085-1088. https://doi.org/10.1029/TR039i006p01085

[3] Nezu, Iehisa. "Experimental study on secondary currents in open channel flows." In *Proc. of 21st IAHR Congress, Melbourne, 1985*, vol. 2, pp. 115-119. 1985.

[4] Nezu, I., H. Nakagawa, and A. Tominaga. "Secondary currents in a straight channel flow and the relation to its aspect ratio." In *Turbulent shear flows 4*, pp. 246-260. Springer, Berlin, Heidelberg, 1985. https://doi.org/10.1007/978-3-642-69996-2_20

[5] Shinneeb, A-M., G. Nasif, and R. Balachandar. "Effect of the aspect ratio on the velocity field of a straight open-channel flow." *Physics of Fluids* 33, no. 8 (2021): 085110. https://doi.org/10.1063/5.0057343

[6] Nezu, Iehisa, and Hiroji Nakagawa. *Turbulence in open-channel flows*. Routledge, 2017. https://doi.org/10.1201/9780203734902

[7] Tominaga, Akihiro, Iehisa Nezu, Kazuhiro Ezaki, and Hiroji Nakagawa. "Three-dimensional turbulent structure in straight open channel flows." *Journal of hydraulic research* 27, no. 1 (1989): 149-173. https://doi.org/10.1080/00221688909499249

[8] Nasif, G., R. Balachandar, and R. M. Barron. "Supercritical flow characteristics in smooth open channels with different aspect ratios." *Physics of Fluids* 32, no. 10 (2020): 105102. https://doi.org/10.1063/5.0021609
[9] Siemens PLM-Global, *STAR-CCM+ V13.06.012*, User Manual, 2018.
[10] Versteeg, H. K., and W. Malalasekera. "An introdution to computational fluid dynamics." *The finite volume method* (1995).
[11] Menter, F. R., and M. Kuntz. "Adaptation of eddy-viscosity turbulence models to unsteady separated flow behind vehicles." In *The aerodynamics of heavy vehicles: trucks, buses, and trains*, pp. 339-352. Springer, Berlin, Heidelberg, 2004. https://doi.org/10.1007/978-3-540-44419-0_30
[12] Travin, Andrey, Michael Shur, Michael Strelets, and P. R. Spalart. "Physical and numerical upgrades in the detached-eddy simulation of complex turbulent flows." In *Advances in LES of complex flows*, pp. 239-254. Springer, Dordrecht, 2002. https://doi.org/10.1007/0-306-48383-1_16
[13] Spalart, Philippe R., Shur Deck, Michael L. Shur, Kyle D. Squires, M. Kh Strelets, and Andrei Travin. "A new version of detached-eddy simulation, resistant to ambiguous grid densities." *Theoretical and computational fluid dynamics* 20, no. 3 (2006): 181-195. https://doi.org/10.1007/s00162-006-0015-0
[14] Wilcox, David C. "Simulation of transition with a two-equation turbulence model." *AIAA journal* 32, no. 2 (1994): 247-255. https://doi.org/10.2514/3.59994
[15] Wilcox, David C. "Turbulence modeling for CFD. La Canada, CA: DCW Industries." Inc, November (2006).
[16] Nasif, G., R. Balachandar, and R. M. Barron. "Influence of bed proximity on the three-dimensional characteristics of the wake of a sharp-edged bluff body." Physics of Fluids 31, no. 2 (2019): 025116. https://doi.org/10.1063/1.5085666
[17] Nasif, G., R. Balachandar, and R. M. Barron. "Effect of gap on the flow characteristics in the wake of a bluff body near a wall." International Journal of Computational Methods and Experimental Measurements 7, no. 4 (2019): 305-315.
https://doi.org/10.2495/CMEM-V7-N4-305-315
[18] Nasif, Ghassan, A-M. Shinneeb, Ram Balachandar, and Chandra Somayaji. "Turbulent Structures in Gap Flow." CFD Letters 14, no. 2 (2022): 24-34.
https://doi.org/10.37934/cfdl.14.2.2434
[19] Nasif, Ghassan Gus. "CFD Simulation of Oil Jets with Application to Piston Cooling." (2014).
[20] Heidari, Mehdi, Ram Balachandar, Vesselina Roussinova, and Ronald M. Barron. "Characteristics of flow past a slender, emergent cylinder in shallow open channels." Physics of Fluids 29, no. 6 (2017): 065111. https://doi.org/10.1063/1.4986563
[21] Spalart, Philippe R., and Craig Streett. Young-person's guide to detached-eddy simulation grids. No. NAS 1.26: 211032. 2001.
[22] Shinneeb, Monsif, Ghassan Nasif, And Ram Balachandar. "Computational Investigation of the Effect of the Aspect Ratio On Secondary Currents in Open Channels." Advances in Fluid Dynamics with emphasis on Multiphase and Complex Flow 132 (2021): 49.
https://doi.org/10.2495/MPF210051
[23] Clauser, Francis H. "Turbulent boundary layers in adverse pressure gradients." Journal of the Aeronautical Sciences 21, no. 2 (1954): 91-108.
https://doi.org/10.2514/8.2938